WATER RESEARCH 47 (2013) 2572–2582

Available online at www.sciencedirect.com

SciVerse ScienceDirect

journal homepage: www.elsevier.com/locate/watres

Sensitivity of the transport and retention of stabilized silver nanoparticles to physicochemical factors

Yan Liang [a], Scott A. Bradford [b,*], Jiri Simunek [c], Harry Vereecken [a], Erwin Klumpp [a]

[a] Agrosphere Institute, IBG-3, Forschungszentrum Jülich GmbH, Jülich, Germany
[b] US Salinity Laboratory, USDA, ARS, Riverside, CA, United States
[c] Department of Environmental Sciences, University of California, Riverside, CA, United States

ARTICLE INFO

Article history:
Received 11 December 2012
Received in revised form
14 February 2013
Accepted 16 February 2013
Available online 26 February 2013

Keywords:
Stabilized silver nanoparticles
Saturated porous media
Time- and depth-dependent retention
Surfactant
Competitive attachment

ABSTRACT

Saturated sand-packed column experiments were conducted to investigate the influence of physicochemical factors on the transport and retention of surfactant stabilized silver nanoparticles (AgNPs). The normalized concentration in breakthrough curves (BTCs) of AgNPs increased with a decrease in solution ionic strength (IS), and an increase in water velocity, sand grain size, and input concentration (C_o). In contrast to conventional filtration theory, retention profiles (RPs) for AgNPs exhibited uniform, nonmonotonic, or hyperexponential shapes that were sensitive to physicochemical conditions. The experimental BTCs and RPs with uniform or hyperexponential shape were well described using a numerical model that considers time- and depth-dependent retention. The simulated maximum retained concentration on the solid phase (S_{max}) and the retention rate coefficient (k_1) increased with IS and as the grain size and/or C_o decreased. The RPs were more hyperexponential in finer textured sand and at lower C_o because of their higher values of S_{max}. Conversely, RPs were nonmonotonic or uniform at higher C_o and in coarser sand that had lower values of S_{max}, and tended to exhibit higher peak concentrations in the RPs at lower velocities and at higher solution IS. These observations indicate that uniform and nonmonotonic RPs occurred under conditions when S_{max} was approaching filled conditions. Nonmonotonic RPs had peak concentrations at greater distances in the presence of excess amounts of surfactant, suggesting that competition between AgNPs and surfactant diminished S_{max} close to the column inlet. The sensitivity of the nonmonotonic RPs to IS and velocity in coarser textured sand indicates that AgNPs were partially interacting in a secondary minimum. However, elimination of the secondary minimum only produced recovery of a small portion (<10%) of the retained AgNPs. These results imply that AgNPs were largely irreversibly interacting in a primary minimum associated with microscopic heterogeneity.

Published by Elsevier Ltd.

1. Introduction

Silver nanoparticles (AgNPs) have been widely used in various commercial products because of their strong antimicrobial activity (Kang et al., 2011). However, generation of AgNP aggregates can lead to a loss of antibacterial activity (Kvitek et al., 2008; Zhang et al., 2012). AgNPs are therefore commonly modified with surfactants or polymers to increase their stability in liquids (Kvitek et al., 2008; Thio et al., 2012; Zhang et al., 2012). AgNPs in consumer products have the

* Corresponding author. Tel.: +1 951 369 4857; fax: +1 951 342 4964.
E-mail address: scott.bradford@ars.usda.gov (S.A. Bradford).
0043-1354/$ – see front matter Published by Elsevier Ltd.
http://dx.doi.org/10.1016/j.watres.2013.02.025

potential to be released into the environment (Benn and Westerhoff, 2008; Geranio et al., 2009). Concentrations of AgNPs were estimated to range between 0.7 and 2.2 μg/kg in sediment, but they can be even higher in sludge-treated soil (Gottschalk et al., 2009). Consequently, there is concern that the antimicrobial effects of released AgNPs may adversely impact ecosystem health (Choi et al., 2010). It has been reported that surface modification of NPs are crucial to determine the fate of NPs in the environment (Kvitek et al., 2008; Tian et al., 2010; Lin et al., 2012; Wang et al., 2012). Knowledge about the processes controlling the subsurface transport and retention of surface modified AgNPs in soils and sediments is therefore critical for accurate exposure assessment and to develop efficient remediation techniques.

Simplified systems are typically employed to determine fundamental mechanisms and models for colloid and NP transport and deposition in the environment. For example, quartz sands or glass beads are normally used as model porous media and monovalent salts are used in electrolyte solutions. Previous studies with quartz sands (Tian et al., 2010; Lin et al., 2011, 2012; Song et al., 2011; Thio et al., 2012) or soils (Sagee et al., 2012) have demonstrated that AgNP transport is sensitive to the surface properties of both AgNPs and porous media, and the chemical composition of solution. The presence of organic matter such as surfactants or humic acid tended to enhance the mobility of AgNPs (Tian et al., 2010; Lin et al., 2012; Thio et al., 2012), while higher ionic strength and divalent cations promoted aggregation and retention (Lin et al., 2011; Thio et al., 2012; Zhang et al., 2012). Other researchers have demonstrated a complex coupling between many physicochemical factors (e.g., grain size, flow velocity, the chemistry of the aqueous and solid phases, organic matter, particle concentration, functionalized surfaces) and the environmental transport of NPs (Jaisi et al., 2008; Liu et al., 2009; Tong et al., 2010; Godinez and Darnault, 2011; Wang et al., 2012). Properties of AgNPs (e.g., surface modification) and the interacting matrices will subsequently influence the dissolution, aging, and transformation (e.g., into silver sulfide NPs) of AgNPs that are released into the environment (Benn and Westerhoff, 2008; Geranio et al., 2009; Kim et al., 2010; Nowack, 2010; Cornelis et al., 2012; Coutris et al., 2012; Levard et al., 2012; Li and Lenhart, 2012).

Filtration theory (Yao et al., 1971) has commonly been employed to predict the influence of physicochemical factors on the mass transfer of NPs to collector surfaces (Jaisi et al., 2008; Liu et al., 2009; Tian et al., 2010). However, deviations have frequently been reported between filtration theory predictions and experimental observations for both NPs and colloids (Adamczyk et al., 1995; Ko and Elimelech, 2000; Tufenkji and Elimelech, 2005). For example, filtration theory predicts an exponential distribution of retained NPs with distance, whereas hyperexponential, uniform, and nonmonotonic retention profiles (RPs) have been commonly reported (Li et al., 2004; Li and Johnson, 2005; Tong et al., 2005; Bradford et al., 2006). A wide variety of factors have been demonstrated to contribute to deviations of RPs between filtration theory predictions and experimental observations including: heterogeneity of the particle and collector surfaces (Tufenkji and Elimelech, 2005), roughness (Kretzschmar et al., 1997), the presence of stabilizing agents (Wang et al., 2012), straining (Li et al., 2004), aggregation (Bradford et al., 2006), and hydrodynamic drag (Li and Johnson, 2005; Johnson et al., 2007). Most previous research has been directed to explain the occurrence and causes of hyperexponential RPs, whereas relatively little attention has been directed at studying nonmonotonic RPs (Tong et al., 2005; Yuan and Shapiro, 2011). To date, no information on RPs for AgNPs has been reported in the literature. The retention of NPs will determine their long-term transport potential, thus information on RPs is essential to predict their fate (Chowdhury et al., 2011).

Filtration theory employs an empirical sticking efficiency (α) to account for the fraction of the NPs that is immobilized on the collector surface. Colloid immobilization is implicitly assumed to occur without further mobilization. In reality, only a small portion of the collector surface may contribute to NP retention under unfavorable attachment conditions (Bradford et al., 2009), and this "favorable" area can change with solution chemistry and velocity (Adamczyk et al., 1995; Ko and Elimelech, 2000). Enhanced retention of colloids and/or NPs occurs at locations associated with surface roughness, grain–grain contacts, and locations of chemical heterogeneities because of lower velocities or increased adhesion (Li et al., 2005; Wang et al., 2011). Particles in unfavorable regions can be slowly transported along the collector surface by hydrodynamic forces to these "favorable" locations (Li et al., 2005; Xu et al., 2008). Particle retention in "favorable" locations will decrease over time as these locations are blocked or filled (Ko and Elimelech, 2000). The rate of filling of these "favorable" locations will depend on the particle concentration. Higher particle concentrations will fill these "favorable" locations more rapidly and thereby increase their transport potential (Bradford et al., 2009; Chowdhury et al., 2011).

The objective of this study is to improve our understanding and ability to simulate the transport and retention of stabilized AgNPs in subsurface environments. This information is needed to assess the risk of groundwater contamination and to improve process descriptions in mathematical models. Saturated packed column experiments were conducted under a variety of ionic strengths, grain sizes, NP concentrations, and flow velocities to systematically investigate physicochemical factors that influence AgNP transport. The collected data and modeling provides valuable insight on the evolution of RP shape for AgNPs and other particles (NPs, colloids, and microorganisms) in porous media, transitioning from hyperexponential to nonmonotonic, and to uniform RPs.

2. Materials and methods

2.1. Solution chemistry and porous media

Electrolyte solutions were made using Milli-Q water and KNO_3. Three solution ionic strengths (IS) were considered, namely: 1, 2.5, and 5 mM KNO_3. These electrolyte solutions were unbuffered, and the pH of influent and effluent ranged from 6 to 7 during the course of the column transport experiments.

Three sizes of quartz sands were employed in the column experiments. The median grain size of these sands are 240, 350 (Quarzwerke GmbH, Germany) and 607 μm (Teco-Sil, CE Minerals Greenville, USA). The sands are reported to consist of

at least 99.7% SiO_2 (quartz) and trace amounts of metal oxides. Additional purification procedures that are described in the Supplementary Information (S1) were applied to control the metal oxide content and organic impurities in the sands, which can limit or enhance NP transport (Lin et al., 2011; Thio et al., 2012). The surface charge characteristics of the clean sand were determined using a Nano-Zetasizer apparatus (Malvern ZetaSizer 4) after it had been crushed to a powder and placed in a selected electrolyte solution.

2.2. AgNPs

AgNP suspensions (10.16% w/w) were produced by chemical precipitation of silver nitrate using an aqueous reduction method (AgPURE™, rent a scientist® GmbH, Germany). The AgNPs were modified using mixture of two stabilizers, 4% w/w each of Polyoxyethylene Glycerol Trioleate and Polyoxyethylene (20) Sorbitan mono-Laurat (Tween 20) (Figure S1, in the Supplementary Information). The total unbounded/free surfactant was around 5% in the original concentrated AgNPs suspension when measured after ultracentrifugation for 6 h. Both of these surfactants are non-ionic and form steric repulsion barriers between AgNPs that help to stabilize the suspension and minimize aggregation. This product corresponds to the OECD reference material NM-300 Silver currently being used for nanomaterial research. Release of Ag^+ from the NM-300 product employed in our study and other research (Kaegi et al., 2011; Klein et al., 2011) was less than 1% of the total mass over three days, which is was much longer than the experiments in this study (<20 h).

The size and morphology of dry AgNPs were measured using a scanning electron microscope (Gemini 1550 VP, Carl Zeiss, Jena, Germany) and a transmission electron microscope (Philips CM 200 FEG). The suspension for each experiment was freshly prepared (to minimize the dissolution of AgNPs) by dilution of the concentrated stock suspension of stabilized AgNPs into selected electrolyte solutions to achieve approximate concentrations of 10, 5, and 1 mg L^{-1} and then sonicated for 15 min in a sonication bath. The final amount of surfactant in the suspension was less than 1×10^{-3} % (W/W) and was proportional to the AgNP concentration. To investigate the presence of free surfactant molecules on AgNPs retention, additional experiments were conducted by adding 10 or 30 mg L^{-1} of the surfactants in the AgNP suspension. The added surfactants were the same as the original surface coating, a mixture of polyoxyethylene glycerol trioleate and Tween 20 at equal concentrations. The Nano-Zetasizer apparatus was also used to determine the size distribution as a function of time and the electrophoretic mobility (EPM) of the AgNPs in different KNO_3 solutions.

2.3. Extended DLVO calculations

Extended DLVO (XDLVO) theory was used to better interpret AgNP deposition in porous media. This theory considers the DLVO interaction energy (sum of electrostatic and van der Waals interactions) and two additional repulsive potentials arising from osmotic (V_{osm}) and elastic (V_{elas}) interactions from the surface coating. The interaction energy barrier calculation is presented in the Supplementary Information (S2).

2.4. Column experiments

Saturated transport experiments were performed in stainless steel columns (3 cm inner diameter, 12 cm length) that were wet-packed with quartz sand. A hydrophilic nylon membrane, which was supported by a steel plate, was used as a capillary barrier and filter at the bottom and top of the column. During packing, the column was vibrated to minimize air entrapment and to ensure homogenous packing. A peristaltic pump was used to inject solutions at a steady Darcy velocity (q = 0.03–0.7 cm min^{-1}) through the column in an upflow mode. A three-way valve was used to switch flow to the column between a D_2O tracer in electrolyte solution, AgNPs suspensions, and particle-free electrolyte solutions.

Before initiating a transport experiment, the packed column was conditioned with around 50 pore volumes of KNO_3 solution. A nonreactive tracer experiment was then conducted by injecting 90 mL of D_2O into the column. The same electrolyte solution and injection velocity were used in D_2O and NP transport experiments in a given column. Column effluent samples (2 mL each) were collected continuously in ultra high performance plastic centrifuge tubes (VWR International GmbH, Germany) using a fraction collector. Tracer D_2O concentrations were quantified by high-performance liquid chromatography (D-7000 HPLC, High-Technologies Corporation, Japan) with a RI detector L-2490. The concentrations of D_2O were evaluated using a calibration curve between the peak area of the RI signal and standard solutions (correlation coefficients were greater than 0.999). The column pore water velocity and dispersivity were obtained by fitting D_2O breakthrough curves (BTCs) to the one-dimensional form of the advective-dispersive transport equation using the CXTFIT code (Toride et al., 1999).Table 1 provides a summary of the column transport properties for all experiments.

After the tracer experiment, a 90 mL pulse of AgNP suspension was injected into the column, followed by flushing with several pore volumes of particle-free electrolyte solution. The electrolyte concentration and flow rate were kept constant during a given experiment. Effluent concentrations of AgNPs were determined from Ag concentrations that were determined by inductively coupled plasma mass spectrometry (ICP-MS, Agilent 7500ce). In brief, AgNPs were treated by 15% HNO_3 to dissolve the particles and to diminish sorption onto the sampling tubes. Solutions were spiked with Rh solution (1 mg L^{-1}) as an internal standard, and diluted as needed before analysis by ICP-MS. Each sample was measured three times and the average value was taken for analysis. After completion of the transport experiments, the porous medium was carefully excavated in 1 cm increments (12 layers). The sand was freeze dried and then digested by HNO_3. The Ag concentration in the HNO_3 digest was again determined by ICP-MS. The AgNPs RPs were subsequently determined from this information and the measured dry mass of sand in each increment.

2.5. Theory and model

Version 4.14 of the HYDRUS-1D computer code (Šimůnek et al., 2008) was used to simulate the transport and retention of stabilized AgNPs in column experiments conducted under various

Table 1 – Experimental parameters and the mass recovery for column experiments.

	d_{50} μm	C_o mg L^{-1}	IS mM	q cm min^{-1}	λ cm	φ	Recovery, %		
							M_{eff}	M_{sand}	M_{total}
Fig. 1	240	10	1	0.7	0.055	0.353	13.9	115.8	129.7
	350	10	1	0.7	0.049	0.403	41.5	52.0	93.5
	607	10	1	0.7	0.056	0.418	45.6	54.1	99.7
Fig. 2	607	10	1	0.7	0.056	0.418	45.6	54.1	99.7
	607	5	1	0.7	0.077	0.429	43.1	44.8	87.9
	607	1	1	0.7	0.089	0.396	17.4	92.5	109.9
Fig. 3	607	10	5	0.7	0.097	0.403	4.6	103.5	108.1
	607	10	2.5	0.7	0.064	0.388	21.8	75.6	97.4
	607	10	1	0.7	0.056	0.418	45.6	54.1	99.7
Fig. S3	350	10	5	0.7	0.038	0.369	5.6	101.4	107.0
	350	10	2.5	0.7	0.044	0.388	11.1	81.0	92.1
	350	10	1	0.7	0.049	0.403	41.5	52.0	93.5
Fig. 4	607	10	1	0.03	0.110	0.427	24.9	73.2	98.1
	607	10	1	0.14	0.045	0.393	27.0	73.2	100.2
	607	10	1	0.35	0.080	0.415	40.1	64.0	104.1
	607	10	1	0.7	0.056	0.418	45.6	54.1	99.7
Fig. 5	607	10	5	0.7	0.097	0.403	4.6	103.5	108.1
	607	10[a]	5	0.7	0.070	0.411	4.5	91.6	96.1
	607	10[b]	5	0.7	0.057	0.428	5.2	96.8	102.0

Fig. 1: grain size effect; Fig. 2: concentration effect; Fig. 3 and Fig. S3: ionic strength effect; Fig. 4: flow rate effect; Fig. 5: surfactant effect; 10[a], 10 mg L^{-1} of AgNPs and 10 mg L^{-1} additional surfactant; 10[b], 10 mg L^{-1} of AgNPs and 30 mg L^{-1} additional surfactant. d_{50}, grain size; C_o, AgNP input concentration; IS, ionic strength; q, Darcy velocity; λ, dispersivity; φ, porosity; M_{eff}, M_{sand}, and M_{total} are mass percentages recovered from effluent, sand, and total, respectively. The value of λ was obtained by fitting tracer BTC, φ was determined gravimetrically.

physicochemical conditions. The aqueous and solid phase mass balance equations for AgNPs are given in this model as:

$$\frac{\partial(\theta_w C)}{\partial t} = \frac{\partial}{\partial z}\left(\theta_w D \frac{\partial C}{\partial z}\right) - \frac{\partial(qC)}{\partial z} - \theta_w \psi k_1 C \quad (1)$$

$$\frac{\partial(\rho_b S)}{\partial t} = \theta_w \psi k_1 C \quad (2)$$

where θ_w[–] is the volumetric water content, C[N_c L^{-3}, N_c and L denote the number of NPs and units of length, respectively] is the aqueous phase AgNP concentration, t is time [T, T denotes time units], z [L] is the distance from the column inlet, D [L^2T^{-1}] is the hydrodynamic dispersion coefficient, q [L T^{-1}] is the Darcy water flux, ψ [–] is a dimensionless function to account for time- and depth-dependent blocking, k_1 [T^{-1}] is the first-order retention coefficient, ρ_b [M L^{-3}, M denote units of mass] is the soil bulk density, and S [N_c M^{-1}] is the solid phase AgNP concentration. The first and second terms on the right hand side of Equation (1) account for dispersive and advective transport of AgNPs, whereas the third term is used to describe NP retention on the solid phase. The pore water velocity and dispersivity values in the AgNP transport simulations were based on values determined from the conservative tracer experiments.

When $\psi = 1$, an exponential distribution of retained AgNPs is predicted with depth. Conversely, ψ can be less than 1 when it is given as (Bradford et al., 2006):

$$\psi = \left(1 - \frac{S}{S_{max}}\right)\left(\frac{d_{50} + z}{d_{50}}\right)^{-\beta} \quad (3)$$

where d_{50} [L] is the median grain size of the porous medium, β [–] is an empirical parameter controlling the shape of the spatial distribution of retained NPs (i.e., the depth dependence of the retention coefficient), and S_{max} [N_c M^{-1}] is the maximum solid phase concentration of deposited AgNPs. The first term on the right side of Equation (3) accounts for time-dependent blocking/filling of retention sites using a Langmuirian approach (Deshpande and Shonnard, 1999). This blocking term implies that retention decreases with time and that the retention profile becomes uniform with depth as S approaches S_{max}. The second term on the right side of Equation (3) describes depth-dependent retention (e.g., a decreasing retention rate with depth). When $\beta = 0$, this term equals 1 and an exponential distribution of retained AgNPs is predicted with depth similar to conventional filtration theory. Conversely, when $\beta > 0$ is employed, then the retention profile of AgNPs exhibits a uniform or hyperexponential shape (e.g., a higher deposition rate close to the column inlet). In this study, a value of $\beta = 0.432$ was employed based on information presented in the literature (Bradford et al., 2003). The AgNP retention model parameters (k_1 and S_{max}) were determined by simultaneously inverse fitting to experimental BTC and RP data using the Levenberg–Marquardt nonlinear least squares optimization algorithm (Marquardt, 1963) in HYDRUS-1D. It should be mentioned that Equations (1)–(3) cannot account for nonmonotonic retention profiles (a peak in retention down gradient from the column inlet) that have sometimes been reported (Li and Johnson, 2005; Tong et al., 2005; Bradford et al., 2006).

3. Results and discussion

3.1. *Characterization of AgNPs*

Figure S2 presents SEM and TEM images of the stabilized AgNPs. These images indicate that the AgNPs were spherical

in shape and had a very narrow size distribution with around 99% of the diameters in the size range of 15–20 nm. The hydrodynamic diameter (d_p) of the AgNPs was measured by DLS to range from 45.1 ± 4.5 to 60.7 ± 14.9 nm when the IS was 1–5 mM and the particle concentration was 10 mg L^{-1}. Measurements of d_p taken over a 24 h period demonstrated that the AgNP suspensions were very stable. Similar size results have been reported in the literature (Klein et al., 2011). The core surface potentials of the AgNPs in 1, 2.5, and 5 mM KNO_3 solutions that were predicted by soft particle theory (Ohshima, 2005) and measurements of electrophoretic mobility are summarized in Table 2. Core surface potentials of AgNPs and clean sand were always negative and did not vary much over the considered range of IS, pH, and C_o (Table 2). The zeta potential of the clean sands was much more negatively charged than that for the AgNPs.

Measured and predicted surface potential information given in Table 2 were used to determine the AgNP–Sand and AgNP–AgNP interaction energies based on XDLVO theory. The maximum van der Waals and electrostatic double layer interaction energy, $(V_{vdW} + V_{ed})_{max}$, predicted for AgNP–sand and AgNP–AgNP slightly decreased with increasing IS (Table 2). A shallow secondary minimum was predicted for both AgNP–sand and AgNP–AgNP interactions. These energies were very weak compared to steric repulsion formed by the adsorbed surfactant layer. Steric interactions arising from the surfactants on the AgNPs contributed significantly to the total energy barriers. Consequently, unfavorable conditions were predicted for AgNP retention and aggregation. However, it should be mentioned that these calculations only considered mean properties of the AgNPs and sand, and do not account for the roles of physical or chemical heterogeneity and grain–grain contacts on AgNP retention. Furthermore, the surfactant coating on AgNPs can also attach to collector surfaces (Lin et al., 2012).

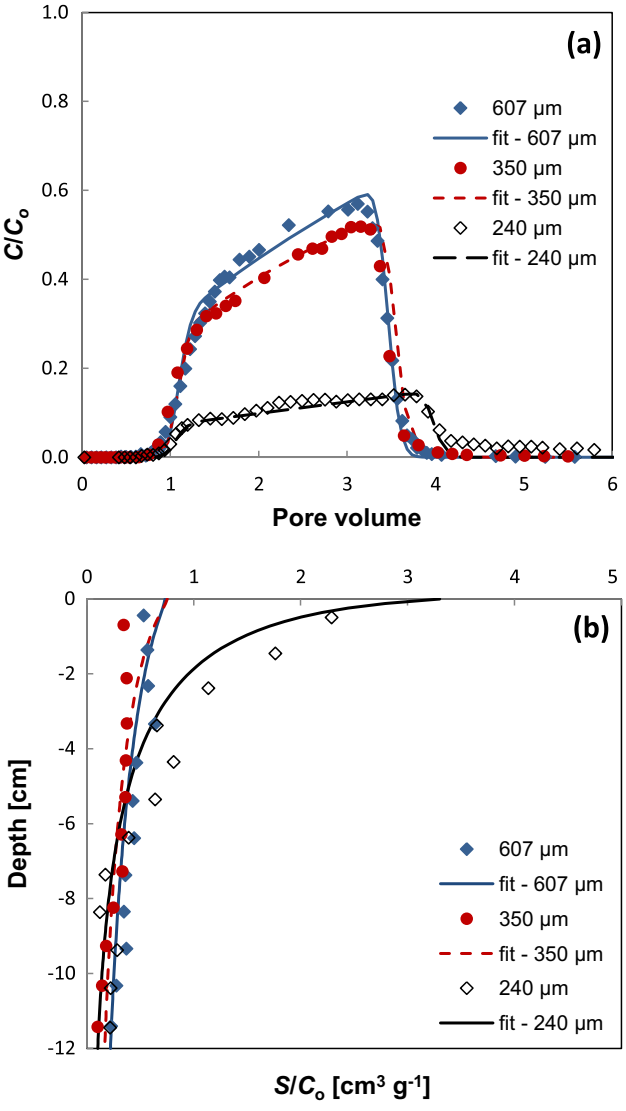

Fig. 1 – Grain size effect: Observed and fitted breakthrough curves (a) and retention profiles (b) of AgNPs in 240, 350 and 607 μm sands, respectively. Other experimental conditions were the same: Electrolyte, 1 mM KNO_3; input concentration, 10 mg L^{-1} AgNPs; Darcy velocity, 0.7 cm/min.

3.2. *Grain size*

In order to investigate the influence of grain size on AgNP mobility, column experiments were conducted in 607, 350, and 240 μm sands when IS = 1 mM, q = 0.7 cm min^{-1}, and C_o = 10 mg L^{-1}. Experimental conditions and the corresponding mass balance information for the BTC, RP, and total column are presented in Table 1. The total column mass balance was >93% and this provides a high degree of confidence in our experimental procedures and protocols. The BTCs are plotted as the normalized effluent concentrations (C/C_o) versus pore volumes. The RPs are plotted as the normalized solid phase concentration (S/C_o) as a function of distance from the column inlet. Observed and simulated BTCs and RPs are shown in Fig. 1. The model simulation successfully captured the gradual ascent trend of the BTCs, and the shape of the RPs.

Table 2 – Extended DLVO parameters of stabilized AgNPs and quartz sand.

IS mM	d_p nm	ζ^a mV	ζ^b mV	$(V_{vdw} + V_{ed})_{max}$ NP–sand kT	$(V_{vdw} + V_{ed})_{max}$ NP–NP kT	V_{Tmax} NP–NP kT	V_{Tmax} NP–Sand kT
1	45.1	−16.9	−55.0	6.31	1.07	1.71×10^4	2.16×10^3
2.5	48.2	−7.5	−55.4	1.40	<0	1.84×10^4	2.29×10^3
5	60.7	−3.2	−55.3	0.31	<0	2.30×10^4	2.89×10^3

IS, ionic strength; d_p, diameter of AgNPs; ζ^a, predicted core surface potential of AgNPs; ζ^b, measured zeta potential of quartz sand; $(V_{vdw} + V_{ed})_{max}$, maximum energy of van der Waals (V_{vdW}) and electrostatic double layer interaction (V_{ed}); V_{Tmax}, maximum of the total XDLVO energy. NP–NP and NP–Sand, the interaction between two nanoparticles and between nanoparticle and grain surface, respectively.

Lower normalized effluent concentrations occur in the BTCs with decreasing sand size (Fig. 1a), especially between the 350 and 240 μm sands. The amount of AgNP retention shown in the RPs (Fig. 1b) was inversely related to their BTCs. Consistent with these observations, fitted values of k_1 increased with decreasing grain size (Table 3). Filtration theory provides an explanation because it predicts that the mass transfer rate to the grain surface increases with decreasing grain size (Yao et al., 1971). However, the shape of the BTCs and RPs was also sensitive to the grain size. This can be explained in part by time-dependent retention processes associated with blocking. Fitted values of S_{max}/C_o increased with decreasing grain size (Table 3) because of its larger surface area. The retention rate declines as retention sites are increasingly occupied by AgNPs (Equation (3)). Consequently, smaller values of S_{max}/C_o in the coarser sands (350 and 607 μm) produce more asymmetric BTCs (Fig. 1a) and more uniform RPs (Fig. 1b) because of stronger blocking (Bradford et al., 2006). The smallest 240 μm sand produced a hyperexponential RP when blocking is less important. In this case, straining is unlikely because the extremely small ratio of d_p/d_{50} is much lower than the reported threshold for straining (Bradford et al., 2002; Li et al., 2004). Alternatively, variations in the pore-scale velocity can provide a viable explanation for this behavior (Bradford et al., 2011a, 2011b). Specifically, hyperexponential RPs occur when the flux adjacent to the solid surface at the column inlet is the dominant mass transfer mechanism of NPs to the grain surface (Bradford et al., 2011a). Pore-scale water flow simulations demonstrate that this flux increases as the grain size decreases (Bradford et al., 2011a).

3.3. Input concentration

Additional transport experiments were conducted to demonstrate the influence of time-dependent retention on AgNP BTCs and RPs. Fig. 2 presents observed and simulated BTCs and RPs for AgNPs in 607 μm sand when the IS = 1 mM KNO_3, $q = 0.7$ cm min^{-1}, and $C_o = 1$, 5, and 10 mg L^{-1}. The normalized BTCs were sensitive to the value of C_o. Higher C_o produced greater recovery of AgNPs in the effluent and more asymmetric BTCs. The amount of AgNPs in the RPs was inversely related to the BTCs, and the shape of the RPs systematically varied with C_o. In particular, the RP was hyperexponential when $C_o = 1$ mg L^{-1}, was nonmonotonic when $C_o = 5$ mg L^{-1}, and approached a uniform distribution when $C_o = 10$ mg L^{-1}.

The model was able to simulate well the BTCs and most of the RPs in Fig. 2 ($R^2 > 0.96$). The value of k_1 increased with decreasing C_o (Table 3). Consequently, this observation suggests that repulsive AgNP–AgNP interactions between mobile and retained NPs hampered AgNP retention on the grain surface at higher values of C_o. Note that the number of AgNP–AgNP collisions is expected to be proportional to C_o. The hyperexponential RP shape at lower values of $C_o = 1$ mg L^{-1} is attributed to pore-scale hydrodynamic at the column inlet as discussed in the previous section. Observed differences in BTCs and RPs with C_o indicate that time-dependent blocking diminished retention with time (Bradford et al., 2009). Furthermore, values of S_{max}/C_o also increased with decreasing C_o (Table 3). In particular, the BTCs were more asymmetric (Fig. 2a) and the RPs were more uniform (Fig. 2b) at a higher C_o because S_{max} filled more rapidly. The observed transition in RP shape from hyperexponential, to nonmonotonic, and to uniform with increases in C_o indicates that blocking contributed to the development of nonmonotonic RPs. However, the model did not capture the nonmonotonic RP shape for the $C_o = 5$ mg L^{-1} data. Consequently, other factors were also involved in the development of the nonmonotonic RP shape. Potential explanations for these observations will be explored below.

3.4. Ionic strength

Transport experiments were conducted at several IS to better understand the nature of the adhesive interaction influencing

Table 3 – Fitted values (k_1 and S_{max}/C_o) of AgNP transport and retention under various experimental conditions.

	d_{50} μm	C_o mg L^{-1}	IS mM	q cm min^{-1}	k_1 min^{-1}	Standard error k_1	S_{max}/C_o cm^3 g^{-1}	Standard error S_{max}/C_o	R^2
Fig. 1	240	10	1	0.7	3.417	0.191	5.320	1.266	0.979
	350	10	1	0.7	1.182	0.020	0.754	0.023	0.969
	607	10	1	0.7	0.855	0.029	0.732	0.027	0.963
Fig. 2	607	10	1	0.7	0.855	0.029	0.732	0.027	0.963
	607	5	1	0.7	1.018	0.047	1.679	0.219	0.975
	607	1	1	0.7	1.683	0.087	6.949	2.524	0.979
Fig. 3	607	10	5	0.7	3.038	0.095	4.439	0.816	0.969
	607	10	2.5	0.7	1.422	0.033	3.593	0.749	0.962
	607	10	1	0.7	0.855	0.029	0.732	0.027	0.963
Fig. S3	350	10	5	0.7	3.378	0.222	23.012	6.456	0.982
	350	10	2.5	0.7	2.859	0.102	3.482	0.751	0.970
	350	10	1	0.7	1.182	0.020	0.754	0.023	0.969
Fig. 4	607	10	1	0.03	0.058	0.001	1.532	0.067	0.952
	607	10	1	0.14	0.356	0.013	1.095	0.048	0.970
	607	10	1	0.35	0.390	0.021	2.017	0.411	0.956
	607	10	1	0.7	0.855	0.029	0.732	0.027	0.963

Fig. 1: grain size effect; Fig. 2: concentration effect; Fig. 3 and Fig. S3: ionic strength effect; Fig. 4: flow rate effect. d_{50}, grain size; C_o, AgNP input concentration; IS, ionic strength; q, Darcy velocity; k_1, the first-order retention coefficient; S_{max}/C_o, normalized maximum solid phase concentration of deposited NPs; R^2, Pearson's correlation coefficient.

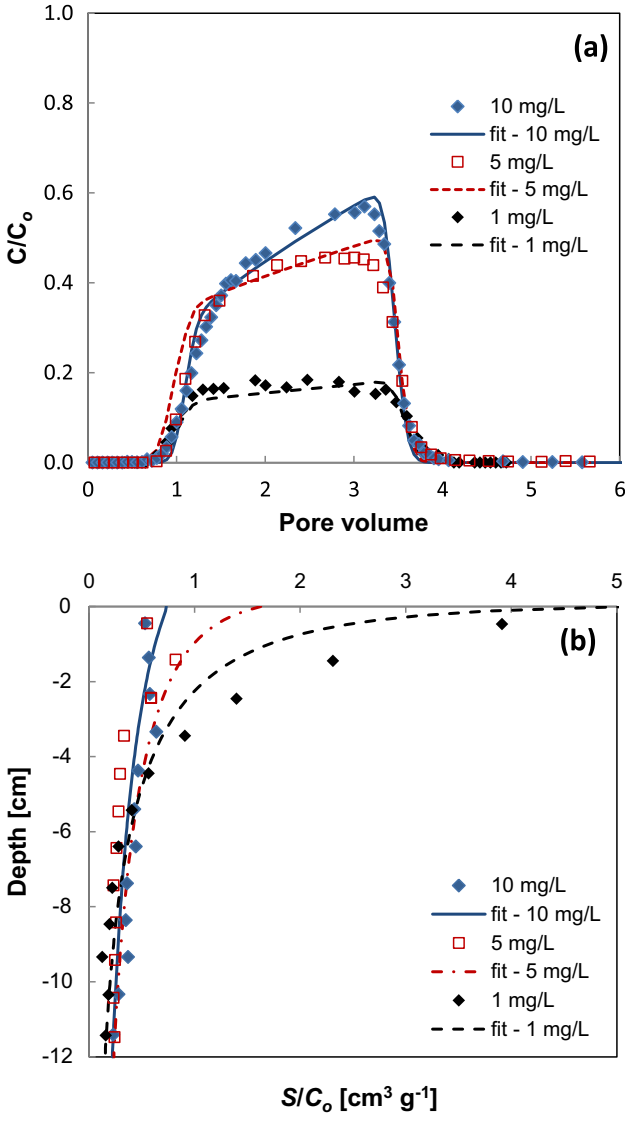

Fig. 2 – Concentration effect: Observed and fitted breakthrough curves (a) and retention profiles (b) of AgNPs under AgNP input concentrations of 1, 5, and 10 mg L^{-1}, respectively. Other experimental conditions were the same: Grain size, 607 μm; electrolyte, 1 mM KNO$_3$; Darcy velocity, 0.7 cm/min.

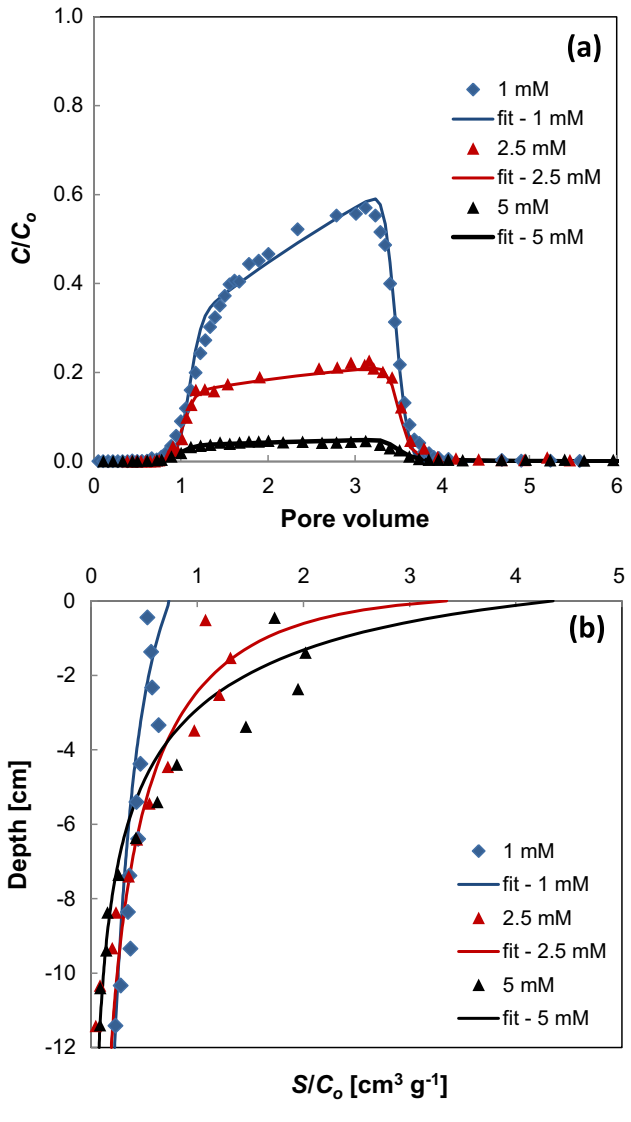

Fig. 3 – Ionic strength effect: Observed and fitted breakthrough curves (a) and retention profiles (b) of AgNPs under 1, 2.5 and 5 mM KNO$_3$, respectively. Other experimental conditions were the same: Grain size, 607 μm; input concentration, 10 mg L^{-1} AgNPs; Darcy velocity, 0.7 cm/min.

AgNP retention. Fig. 3 presents observed and simulated BTCs and RPs of AgNPs in 607 μm quartz sand when $q = 0.7$ cm min^{-1}, $C_o = 10$ mg L^{-1}, and IS = 1, 2.5, and 5 mM KNO_3. Figure S3 provides similar information but in 350 μm quartz sand. For a given sand size, increases in IS produced a significant decline of AgNPs transport and a corresponding increase in retention. This observed trend is consistent with compression of the electrostatic double layer surrounding the collectors at higher IS as reported in previous studies (Jaisi et al., 2008; Lin et al., 2011). The BTCs were well described using the model ($R^2 > 0.96$), whereas the nonmonotonic RP was not accurately simulated.

The sensitivity of BTCs and RPs to IS provides further insight on AgNP retention. BTCs were more asymmetric at the lowest IS = 1 mM and RPs were nonmonotonic when the IS equaled 2.5 or 5 mM. The increase of IS from 1 to 5 mM resulted in an increase of nearly 4-fold on k_1 and around 6-fold on S_{max} (Table 3). Consequently, BTCs were asymmetric and RPs were uniform with depth when IS = 1 mM because the smaller S_{max} was filled rapidly. Conversely, when the IS = 2.5 and 5 mM, values of S_{max} were larger, and the RPs were nonmonotonic because it took longer to fill these regions of the solid surface. Similar behavior occurred at higher IS and in the finer textured 350 μm sand, but in this case the value of S_{max} and the filling times were even larger. The nonmonotonic RPs were therefore more pronounced in the finer sand and at higher IS (2.5 and 5 mM) conditions.

XDLVO calculations predict a shallow secondary minima and significant energy barriers to attachment under these IS

conditions (Table 2). An additional experiment at IS = 5 mM was conducted to verify the role of the secondary minima. After application of AgNPs and rinsing with background particle-free electrolyte solution (around 8 pore volumes in total), the column was flushed with several pore volumes of Milli Q water to expand the double layer thickness and to eliminate the secondary minimum (Figure S4). A pulse of AgNPs was released into the effluent (C/C_o was approximately 0.4) when the secondary minimum was eliminated. However, integration of this pulse indicated that it only accounted for around 7% of the retained mass. This observation suggests that most of the retained AgNP mass was interacting in a primary minimum as a result of physical and/or chemical heterogeneity. Values of k_1 and S_{max} mainly determine the amount of AgNP retention, and both these parameters were lowest at IS of 1 mM. The effect of microscopic heterogeneity on k_1 and S_{max} has been reported to increase with IS because of a smaller zone of electrostatic influence when the double layer is compressed (Torkzaban et al., 2008). Consequently, increasing values of k_1 and S_{max} with IS (Table 3) are therefore expected to largely reflect the effects of microscopic heterogeneity.

3.5. *Flow velocity*

A series of experiments were performed under various flow velocities in 607 μm sand at an IS = 1 mM KNO_3 to further investigate the influence of system hydrodynamics on AgNP fate. Our results demonstrated an increased mass removal of AgNPs with decreasing flow rate (Fig. 4). Higher effluent concentrations and significantly less retention occurred when the flow velocity increased from 0.03 to 0.7 cm min^{-1}. The RPs were nonmonotonic when Darcy velocities were 0.03, 0.14, and 0.35 cm min^{-1}.

Hydrodynamics may affect AgNPs transport and retention in 3 ways by influencing: (i) the rate of mass transfer from the bulk phase to the solid phase (Yao et al., 1971); (ii) the value of S_{max} that is associated with a secondary minimum (Li et al., 2005; Torkzaban et al., 2008); and (iii) the migration rate of particles adjacent to the solid phase (Ko and Elimelech, 2000; Bradford et al., 2011a, 2011b). Each of these factors will be briefly discussed below. In filtration theory, physico–chemical interactions are assumed to control the rate of AgNP mass transfer to the solid surface. The values of $k_1$obtained from the model all increased with increasing velocity (Table 3), consistent with expected trends for the bulk mass transfer rate predicted by filtration theory (Yao et al., 1971; Logan et al., 1995). Conversely, a systematic decrease in S_{max} with increasing velocity was not observed (S_{max}/C_o ranged from 0.732 to 2.017 $cm^3\ g^{-1}$) as would be predicted from torque balance considerations for AgNPs interacting by a secondary minimum. However, S_{max} was found to be lowest at the highest velocity. These observations highlight the relatively insignificant role of secondary minimum interactions for AgNPs and the importance of primary minimum interactions as a result of physical and/or chemical heterogeneity. Furthermore, systematic trends in the RP shape with velocity were not very apparent in Fig. 4b as would be expected if solid phase AgNP migration occurred over long distances. Consequently, the amount of retention in the RPs (Fig. 4b) was

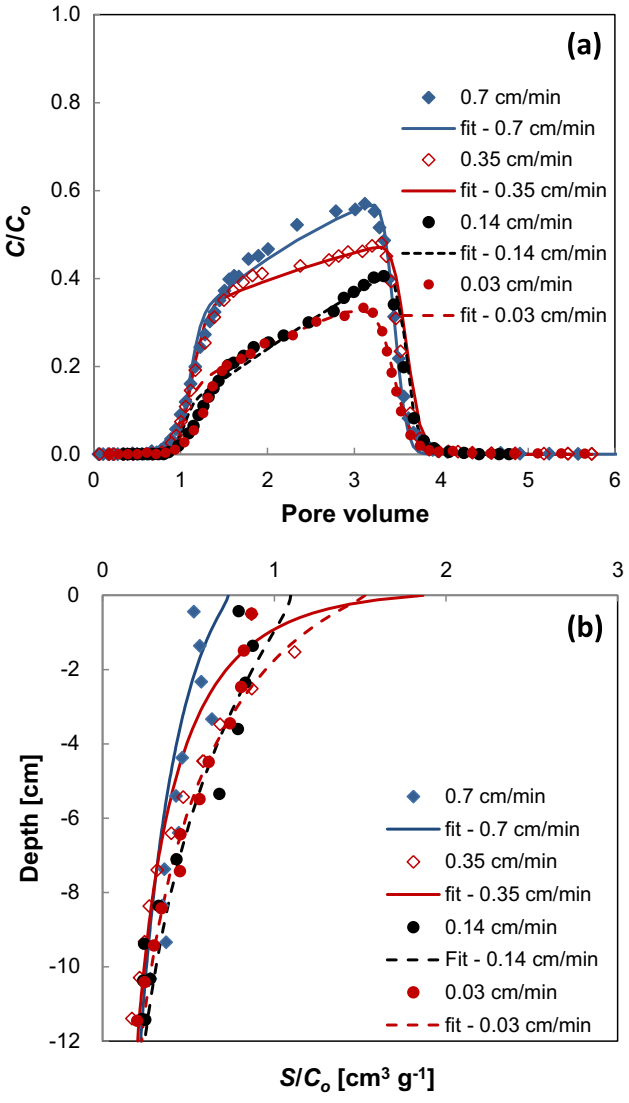

Fig. 4 – Flow rate effect: Observed and fitted breakthrough curves (a) and retention profiles (b) of AgNPs under Darcy velocities of 0.03, 0.14, 0.35, and 0.7 cm/min, respectively. Other conditions were the same: Grain size, 607 μm; electrolyte, 1 mM KNO_3; input concentration, 10 mg L^{-1} AgNPs.

primarily determined by differences in the bulk phase mass transfer rate, and the shape of the RPs was mainly influenced by blocking of S_{max} arising from microscopic heterogeneities.

3.6. *Nonmonotonic RPs*

The above information indicated that the nonmonotonic RPs were strongly linked to blocking behavior. One potential explanation is due to the free surfactants (previously exist or desorption from the stabilized AgNPs) that subsequently adsorbed onto porous media. The RP shape may be altered by surfactant and NP competition for attachment sites that diminishes S_{max} (Lin et al., 2012; Wang et al., 2012). Additional transport experiments with AgNPs in the presence of 10 and

30 mg L^{-1} of surfactants were therefore conducted to test this hypothesis. Other experimental conditions were a grain size of 607 μm, an IS of 5 mM KNO_3, a Darcy velocity equal to 0.7 cm min^{-1}, and $C_o = 10$ mg L^{-1} AgNPs. The BTCs and RPs are shown in Fig. 5. Note that increasing the surfactant concentration had a relatively minor influence on the BTCs and produced nearly the same recoveries from effluent (Table 3), but a large effect on the nonmonotonic RPs. In particular, higher surfactant concentrations were associated with nonmonotonic RPs having peak concentrations at greater distances. The decreasing amount of AgNPs retention near the column inlet with increasing surfactant concentration is therefore likely a result of surfactant adsorption onto the grain that fills the retention sites and then decreases S_{max} at this location. Consequently, the nonmonotonic RPs were determined by the combined influence of time- and depth-dependent retention (described by k_1 and S_{max}), and the effect of surfactant adsorption on S_{max}. The surfactant effect also provides a good explanation for the RPs showed in Fig. 2b. The amount of surfactant in the solution is expected to be proportional to C_o, so the effects of surfactants on AgNP retention are expected to increase with C_o because blocking is more important. In the case of nonmonotonic RPs in Figs. 3b and 4b, the competitive retention of AgNPs and surfactants are also likely to play an important role.

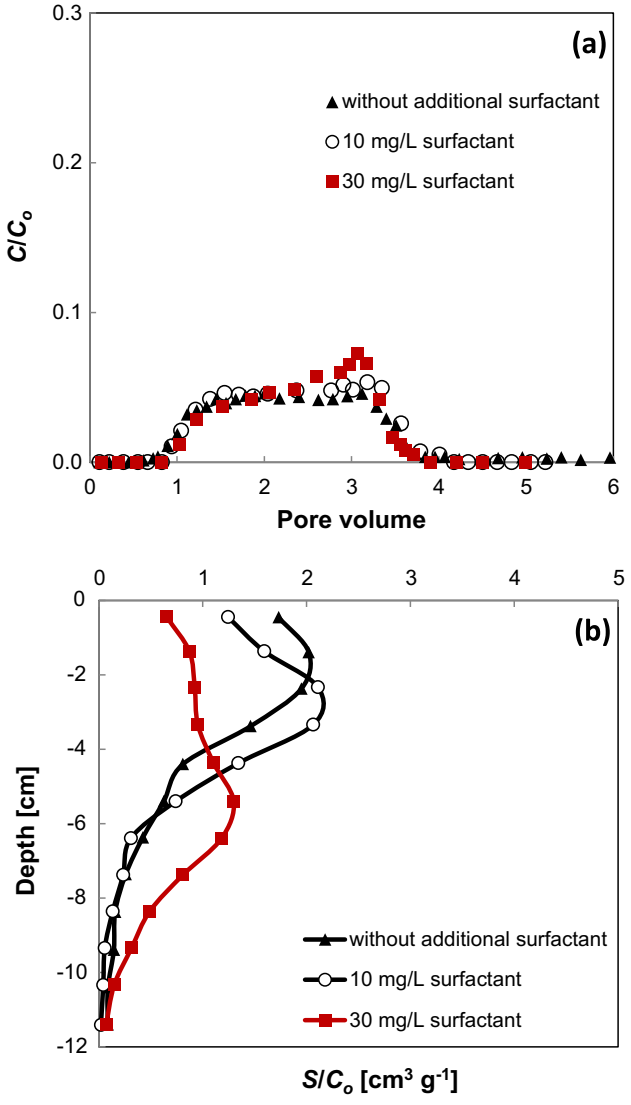

Fig. 5 – Surfactant effect: Observed breakthrough curves (a) and retention profiles (b) of AgNPs without additional surfactant and with adding 10 or 30 mg L^{-1} surfactant in the injected AgNPs suspension, respectively. Other experimental conditions were the same: Grain size, 607 μm; electrolyte, 5 mM KNO_3; input concentration, 10 mg L^{-1} AgNPs; Darcy velocity, 0.7 cm/min.

4. Conclusions

The transport of AgNPs was enhanced with an increase in water velocity, sand grain size, and AgNP input concentration, and a decrease in solution ionic strength. AgNPs were found to mainly interact in irreversible primary minimum as a result of microscopic heterogeneity and partially in a reversible secondary minimum at higher IS. Consequently, the effects of flow velocity on AgNP retention were primarily controlled by the rate of mass transfer to the solid surface. Significantly, the RPs were found to transition from hyperexponential, to nonmonotonic, and to uniform with depth due to the combined effects of hydrodynamics near the column inlet and time-dependent blocking of S_{max} that was influenced by the amounts of surfactants. In particular, the high sensitivity of AgNP retention to the stabilizing agent indicates that artificial stabilizers or natural occurring organic matter will likely facilitate NP transport deeper into the subsurface environment and increase the potential risk of groundwater contamination. Highly idealized systems (clean quartz sand and monovalent electrolyte solutions) were employed in this research to better understand mechanisms of AgNP retention. Additional research is warranted to fully address the transport complexities of natural environments.

Acknowledgments

The first author thanks to the China Scholarship Council (CSC) for financial support. This research was funded by the NanoFlow project supported by German Federal Ministry of Education and Research (BMBF). The authors would like to acknowledge the assistance of Astrid Zimmermann (ZCH, Forschungszentrum Jülich GmbH, Germany) for ICP-MS measurement and Marc Heggen (PGI-5, and ER-C, Forschungszentrum Jülich GmbH, Jülich, Germany) for TEM measurement. Thanks to Herbert Philipp for the technical assistance and Stephan Köppchen for analysis of D_2O samples. The authors also thank Dr. Roy Kasteel for his valuable suggestions for modeling.

Appendix A. Supplementary data

Supplementary data related to this article can be found at http://dx.doi.org/10.1016/j.watres.2013.02.025.

REFERENCES

Adamczyk, Z., Siwek, B., Szyk, L., 1995. Flow-induced surface blocking effects in adsorption of colloid particles. Journal of Colloid and Interface Science 174 (1), 130–141.

Benn, T.M., Westerhoff, P., 2008. Nanoparticle silver released into water from commercially available sock fabrics. Environmental Science & Technology 42 (11), 4133–4139.

Bradford, S.A., Yates, S.R., Bettahar, M., Simunek, J., 2002. Physical factors affecting the transport and fate of colloids in saturated porous media. Water Resources Research 38 (12), 1327.

Bradford, S.A., Simunek, J., Bettahar, M., van Genuchten, M.T., Yates, S.R., 2003. Modeling colloid attachment, straining, and exclusion in saturated porous media. Environmental Science & Technology 37 (10), 2242–2250.

Bradford, S.A., Simunek, J., Walker, S.L., 2006. Transport and straining of *E. coli* O157:H7 in saturated porous media. Water Resources Research 42 (12), W12S12.

Bradford, S.A., Kim, H.N., Haznedaroglu, B.Z., Torkzaban, S., Walker, S.L., 2009. Coupled factors influencing concentration-dependent colloid transport and retention in saturated porous media. Environmental Science & Technology 43 (18), 6996–7002.

Bradford, S.A., Torkzaban, S., Simunek, J., 2011a. Modeling colloid transport and retention in saturated porous media under unfavorable attachment conditions. Water Resources Research 47 (10), W10503.

Bradford, S.A., Torkzaban, S., Wiegmann, A., 2011b. Pore-scale simulations to determine the applied hydrodynamic torque and colloid immobilization. Vadose Zone Journal 10 (1), 252–261.

Choi, O., Yu, C.-P., Esteban Fernández, G., Hu, Z., 2010. Interactions of nanosilver with Escherichia coli cells in planktonic and biofilm cultures. Water Research 44 (20), 6095–6103.

Chowdhury, I., Hong, Y., Honda, R.J., Walker, S.L., 2011. Mechanisms of TiO_2 nanoparticle transport in porous media: role of solution chemistry, nanoparticle concentration, and flowrate. Journal of Colloid and Interface Science 360 (2), 548–555.

Cornelis, G., DooletteMadeleine Thomas, C., McLaughlin, M.J., Kirby, J.K., Beak, D.G., Chittleborough, D., 2012. Retention and dissolution of engineered silver nanoparticles in natural soils. Soil Science Society of America Journal 76 (3), 891–902.

Coutris, C., Joner, E.J., Oughton, D.H., 2012. Aging and soil organic matter content affect the fate of silver nanoparticles in soil. Science of The Total Environment 420 (0), 327–333.

Deshpande, P.A., Shonnard, D.R., 1999. Modeling the effects of systematic variation in ionic strength on the attachment kinetics of Pseudomonas fluorescens UPER-1 in saturated sand columns. Water Resources Research 35 (5), 1619–1627.

Geranio, L., Heuberger, M., Nowack, B., 2009. The behavior of silver nanotextiles during washing. Environmental Science & Technology 43 (21), 8113–8118.

Godinez, I.G., Darnault, C.J.G., 2011. Aggregation and transport of nano-TiO_2 in saturated porous media: effects of pH, surfactants and flow velocity. Water Research 45 (2), 839–851.

Gottschalk, F., Sonderer, T., Scholz, R.W., Nowack, B., 2009. Modeled environmental concentrations of engineered nanomaterials (TiO_2, ZnO, Ag, CNT, Fullerenes) for different regions. Environmental Science & Technology 43 (24), 9216–9222.

Jaisi, D.P., Saleh, N.B., Blake, R.E., Elimelech, M., 2008. Transport of single-walled carbon nanotubes in porous media: filtration mechanisms and reversibility. Environmental Science & Technology 42 (22), 8317–8323.

Johnson, W.P., Li, X., Assemi, S., 2007. Deposition and re-entrainment dynamics of microbes and non-biological colloids during non-perturbed transport in porous media in the presence of an energy barrier to deposition. Advances in Water Resources 30 (6–7), 1432–1454.

Kaegi, R., Voegelin, A., Sinnet, B., Zuleeg, S., Hagendorfer, H., Burkhardt, M., Siegrist, H., 2011. Behavior of metallic silver nanoparticles in a pilot wastewater treatment plant. Environmental Science & Technology 45 (9), 3902–3908.

Kang, K., Lim, D.-H., Choi, I.-H., Kang, T., Lee, K., Moon, E.-Y., Yang, Y., Lee, M.-S., Lim, J.-S., 2011. Vascular tube formation and angiogenesis induced by polyvinylpyrrolidone-coated silver nanoparticles. Toxicology Letters 205 (3), 227–234.

Kim, B., Park, C.-S., Murayama, M., Hochella, M.F., 2010. Discovery and characterization of silver sulfide nanoparticles in final sewage sludge products. Environmental Science & Technology 44 (19), 7509–7514.

Klein, C.L., Comero, S., Locoro, G., Gawlik, B.M., Stahlmecke, B., Romazanov, J., Kuhlbusch, T.A.J., 2011. NM-series of Representative Manufactured Nanomaterials NM-300 Silver Characterisation, Stability, Homogeneity. EUR 24693 EN. Joint Research Centre – Institute for Health and Consumer Protection.

Ko, C.-H., Elimelech, M., 2000. The "Shadow effect" in colloid transport and deposition dynamics in granular porous media: measurements and mechanisms. Environmental Science & Technology 34 (17), 3681–3689.

Kretzschmar, R., Barmettler, K., Grolimund, D., Yan, Y.-D., Borkovec, M., Sticher, H., 1997. Experimental determination of colloid deposition rates and collision efficiencies in natural porous media. Water Resources Research 33 (5), 1129–1137.

Kvitek, L., Pancek, A., Soukupova, J., Kolar, M., Vecerova, R., Prucek, R., Holecova, M., Zboril, R., 2008. Effect of surfactants and polymers on stability and antibacterial activity of silver nanoparticles (NPs). Journal of Physical Chemistry C 112 (15), 5825–5834.

Levard, C., Hotze, E.M., Lowry, G.V., Brown, G.E., 2012. Environmental transformations of silver nanoparticles: impact on stability and toxicity. Environmental Science & Technology 46 (13), 6900–6914.

Li, X., Johnson, W.P., 2005. Nonmonotonic variations in deposition rate coefficients of microspheres in porous media under unfavorable deposition conditions. Environmental Science & Technology 39 (6), 1658–1665.

Li, X., Lenhart, J.J., 2012. Aggregation and dissolution of silver nanoparticles in natural surface water. Environmental Science & Technology 46 (10), 5378–5386.

Li, X., Scheibe, T.D., Johnson, W.P., 2004. Apparent decreases in colloid deposition rate coefficients with distance of transport under unfavorable deposition conditions: a general phenomenon. Environmental Science & Technology 38 (21), 5616–5625.

Li, X., Zhang, P., Lin, C.L., Johnson, W.P., 2005. Role of hydrodynamic drag on microsphere deposition and re-entrainment in porous media under unfavorable conditions. Environmental Science & Technology 39 (11), 4012–4020.

Lin, S., Cheng, Y., Bobcombe, Y., Jones, K.L., Liu, J., Wiesner, M.R., 2011. Deposition of silver nanoparticles in geochemically heterogeneous porous media: predicting affinity from surface composition analysis. Environmental Science & Technology 45 (12), 5209–5215.

Lin, S., Cheng, Y., Liu, J., Wiesner, M.R., 2012. Polymeric coatings on silver nanoparticles hinder autoaggregation but enhance attachment to uncoated surfaces. Langmuir 28 (9), 4178–4186.

Liu, X., O'Carroll, D.M., Petersen, E.J., Huang, Q., Anderson, C.L., 2009. Mobility of multiwalled carbon nanotubes in porous media. Environmental Science & Technology 43 (21), 8153–8158.

Logan, B., Jewett, D., Arnold, R., Bouwer, E., O'Melia, C., 1995. Clarification of clean-bed filtration models. Journal of Environmental Engineering 121 (12), 869–873.

Marquardt, D.W., 1963. An algorithm for least-squares estimation of nonlinear parameters. Journal of the Society for Industrial and Applied Mathematics 11 (2), 431–441.

Nowack, B., 2010. Nanosilver revisited downstream. Science 330 (6007), 1054–1055.

Ohshima, H., 2005. Approximate expression for the electrophoretic mobility of a spherical colloidal particle covered with an ion-penetrable uncharged polymer Layer. Colloid & Polymer Science 283 (8), 819–825.

Sagee, O., Dror, I., Berkowitz, B., 2012. Transport of silver nanoparticles (AgNPs) in soil. Chemosphere 88 (5), 670–675.

Šimůnek, J., Genuchten, M.T.V., Šejna, M., 2008. Development and applications of the HYDRUS and STANMOD software packages, and related codes. Vadose Zone Journal 7 (2), 587–600.

Song, J.E., Phenrat, T., Marinakos, S., Xiao, Y., Liu, J., Wiesner, M.R., Tilton, R.D., Lowry, G.V., 2011. Hydrophobic interactions increase attachment of gum Arabic- and PVP-coated Ag nanoparticles to hydrophobic surfaces. Environmental Science & Technology 45 (14), 5988–5995.

Thio, B.J.R., Montes, M.O., Mahmoud, M.A., Lee, D.-W., Zhou, D., Keller, A.A., 2012. Mobility of capped silver nanoparticles under environmentally relevant conditions. Environmental Science & Technology 46 (13), 6985–6991.

Tian, Y.A., Gao, B., Silvera-Batista, C., Ziegler, K.J., 2010. Transport of engineered nanoparticles in saturated porous media. Journal of Nanoparticle Research 12 (7), 2371–2380.

Tong, M., Li, X., Brow, C.N., Johnson, W.P., 2005. Detachment-influenced transport of an adhesion-deficient bacterial strain within water-reactive porous media. Environmental Science & Technology 39 (8), 2500–2508.

Tong, M.P., Ding, J.L., Shen, Y., Zhu, P.T., 2010. Influence of biofilm on the transport of fullerene (C-60) nanoparticles in porous media. Water Research 44 (4), 1094–1103.

Toride, N., Leij, F.J., van Genuchten, M.T., 1999. The CXTFIT Code for Estimating Transport Parameters from Laboratory or Field Tracer Experiments. Version 2.1. U.S. Salinity Laboratory, USDA-ARS, Riverside, CA. Research Rep. 137.

Torkzaban, S., Tazehkand, S.S., Walker, S.L., Bradford, S.A., 2008. Transport and fate of bacteria in porous media: coupled effects of chemical conditions and pore space geometry. Water Resources Research 44 (4), W04403.

Tufenkji, N., Elimelech, M., 2005. Breakdown of colloid filtration theory: role of the secondary energy minimum and surface charge heterogeneities. Langmuir 21 (3), 841–852.

Wang, D., Paradelo, M., Bradford, S.A., Peijnenburg, W.J.G.M., Chu, L., Zhou, D., 2011. Facilitated transport of Cu with hydroxyapatite nanoparticles in saturated sand: effects of solution ionic strength and composition. Water Research 45 (18), 5905–5915.

Wang, Y., Li, Y., Costanza, J., Abriola, L.M., Pennell, K.D., 2012. Enhanced mobility of fullerene (C60) nanoparticles in the presence of stabilizing agents. Environmental Science & Technology 46 (21), 11761–11769.

Xu, S.P., Liao, Q., Saiers, J.E., 2008. Straining of nonspherical colloids in saturated porous media. Environmental Science & Technology 42 (3), 771–778.

Yao, K.-M., Habibian, M.T., O'Melia, C.R., 1971. Water and waste water filtration. Concepts and applications. Environmental Science & Technology 5 (11), 1105–1112.

Yuan, H., Shapiro, A.A., 2011. A mathematical model for non-monotonic deposition profiles in deep bed filtration systems. Chemical Engineering Journal 166 (1), 105–115.

Zhang, H., Smith, J.A., Oyanedel-Craver, V., 2012. The effect of natural water conditions on the anti-bacterial performance and stability of silver nanoparticles capped with different polymers. Water Research 46 (3), 691–699.